IOP Publishing Journal of Physics: Condensed Matter
J. Phys.: Condens. Matter **32** (2020) 225301 (9pp) https://doi.org/10.1088/1361-648X/ab73a0

Novel porous aluminum nitride monolayer: a first-principles study

Yanwei Luo[1], **Jiahui Hu**[1] **and Yu Jia**[2]

[1] College of Science, Henan University of Technology, Zhengzhou, People's Republic of China
[2] International Laboratory for Quantum Functional Materials, Zhengzhou University, Zhengzhou, People's Republic of China

E-mail: luoyanwei@haut.edu.cn

Received 9 August 2019, revised 22 January 2020
Accepted for publication 5 February 2020
Published 3 March 2020

Abstract

Using *ab initio* calculations within the density functional theory, we explored the possible structures and properties of porous AlN monolayer materials. Two kinds of porous AlN monolayers (H- and T-) are identified. The phonon dispersion spectra together with the *ab initio* molecular dynamics simulations demonstrate that these structures are stable. We further show that the H- and T-AlN porous monolayers have well-defined porous nanostructures and high specific surface areas of 2863 $m^2\ g^{-1}$ and 2615 $m^2\ g^{-1}$ respectively, which is comparable to graphene (2630 $m^2\ g^{-1}$), and can be maintained stably at high temperatures (>1300 K). Furthermore, both porous monolayers exhibit semiconductor properties, with indirect band gaps of 2.89 eV and 2.86 eV respectively. In addition, the electronic structures of the porous monolayers can be modulated by strain. The band gap of porous T-AlN monolayer experiences an indirect–direct transition when biaxial strain is applied. A moderate −9% compression can trigger this gap transition. These results indicate that porous AlN monolayers may potentially be used in future optoelectronic and catalyst applications.

Keywords: aluminum nitride, electronic structure, dynamic stability, *ab initio* calculations

(Some figures may appear in colour only in the online journal)

1. Introduction

The discovery of a variety of two-dimensional (2D) materials, such as graphene [1], phosphorene, transition metal dichalcogenides, and tellurene, has attracted much attention because of their novel electronic and optical properties and their potential applications in nanodevices and nanotechnology [2–7]. Many 2D materials with novel structures, as well as electronic and optical properties, have been theoretically explored and experimentally studied in tandem with the development of experimental synthesis and theoretical analysis techniques [8–12]. One interesting finding in these studies is that the performance of 2D materials can be enhanced dramatically by introducing porous structures [13–18].

The first discovered 2D monolayer material, graphene, was also the first 2D material for which a porous structure was discovered and studied. In 2009, Bieri and coworkers fabricated porous graphene with a regular distribution of the pores [19]. Their study showed that the unique structure of porous graphene leads to properties, such as a wide bandgap and large surface area, which differ from those of graphene. It was therefore proposed as an ideal material for gas purification and energy storage. A new 2D tetra-symmetrical carbon which possesses a high Fermi velocity and Dirac-like fermions similar to graphene was systematically investigated by Liu *et al* [20]. Meanwhile, another 2D material, hexagonal boron nitride (h-BN) has also been studied. For instance, two types of porous BN materials were found by using first-principles calculations and a global structural search method. The calculations showed that these porous BN materials are direct band gap semiconductors and can be used in photonic and optoelectronic devices, and for hydrogen storage [21]. Besides, Wen *et al* predicted a novel polymorph of BN with a body-centered tetragonal structure from *ab initio* calculations [22], and Ma *et al* predicted BN with a Pnma structure [23]. Recently, a series of 2D porous allotropes with a novel octagonal tiling structure was studied by Li *et al* [24]. All the 2D allotropes compounded with group V elements can exist

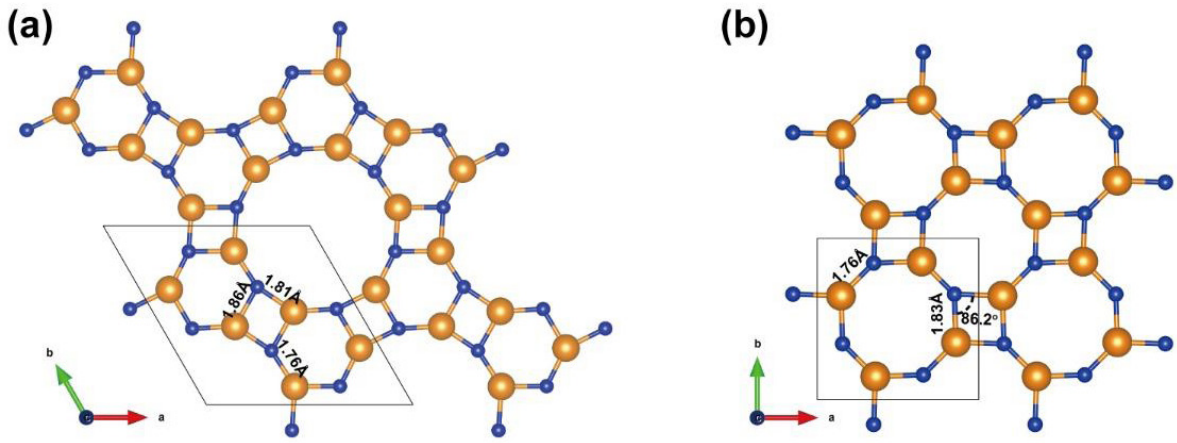

Figure 1. The geometric structures of two AlN monolayers: (a) H-AlN and (b) T-AlN phase. The blue and golden balls represent N and Al atoms, respectively.

stably and possess semiconducting band gaps. Due to their wide band gaps ranging from 0.3 to 2.0 eV, these porous materials can be used in visible and near infrared optoelectronic devices.

As a new and typical 2D III-nitride material, aluminum nitride (AlN) [25, 26] has attracted explosive interest among researchers due to its many intriguing physical properties such as high chemical stability and thermal conductivity, excellent mechanical properties, and significant potential applications [27–30]. Interestingly, high purity AlN monolayer films have been synthesized by conventional growth methods [31–35]. All these experimental and theoretical progress have evoked significant interest in porous AlN monolayers. Monolayer AlN is a typical III-nitride 2D material with the same number of valence electrons in its unit cell as BN. It is thus natural to study the similar porous structures of AlN monolayers.

In this paper, two kinds of porous AlN monolayer are explored by employing *ab initio* calculations using density functional theory. For each structure, the geometric, energetic, and electronic properties are systematically investigated, and their stabilities are analyzed through their phonon dispersion spectra and molecular dynamics simulations. Furthermore, the relationship between the electronic structure and the in-layer strain of each porous monolayer type is also examined.

2. Computational method

All the first-principles calculations in this work were performed by using Vienna *ab initio* simulation package (VASP) [36, 37], which implements the density functional theory (DFT) framework. The projected augmented wave (PAW) method [38] combined with the generalized gradient approximation (GGA) proposed by Perdew, Burke, and Ernzerhof (PBE) [39] was selected to treat the exchange-correlation interactions between electrons. In order to achieve the required accuracy for the electronic properties, the plane-wave expansion cutoff energy was set at 500 eV, and a $21 \times 21 \times 1$ k-point mesh was adopted for the Brillouin zone (BZ) sampling by the Monkhorst–Pack method. A vacuum layer of approximately 25 Å perpendicular to the monolayer was found to be sufficient to prevent interactions between the periodic cells. All the atoms were fully relaxed until the total energy and the residue forces on each atom were converged to 10^{-4} eV and 0.01 eV Å^{-1}, respectively. The Heyd–Scuseria–Ernzerhof (HSE06) functional with 25% Hartree–Fock exchange energy was used in addition to the PBE functional for the hybrid-DFT calculations to evaluate the band gaps of the porous structures more accurately.

3. Results and discussion

3.1. Porous structure and stability

The most common minimum energy structures of 2D monolayer materials are the planar and buckled structures [24]. For example, graphene has a planar structure and silicene has a buckled structure. We consider here AlN monolayer structures with two different geometrical units that we call the H- and T-types, as shown in figure 1. The graphene-like AlN monolayer (g-AlN) was first studied and compared with previous results to test the correction and reliability of our calculations. The lattice constant and bond length are 3.128 Å and 1.806 Å respectively for monolayer g-AlN, which agree with the values of 3.126 Å and 1.80 Å obtained in previous studies [40, 41]. The lattice constants of bulk Wurtzite AlN (WZ-AlN) were also studied and the calculated results ($a = b = 3.11$ Å, $c = 4.99$ Å) agree with previous experimental and theoretical work [28, 42]. After geometry relaxation, the initial structures of H- and T-AlN monolayers became planar ones. Thereby, AlN monolayers have only planar structures, differing from porous graphene which has both planar and buckled structures.

From figure 1(a), we can see that the planar H-AlN structure can be described by the plane group 175.P6/M(C6H-1) with a lattice constant of 8.51 Å. Each hexagonal cell contains six Al atoms and six N atoms. The T-AlN structure can be described by the plane group 127.P4/MBM(D4H-5). The lattice constant is 6.18 Å with each tetragonal cell containing four Al atoms and four N atoms. For clearer presentation, we label the Al–N bond lengths and the angles in figure 1. For the H-AlN structure, each unit cell is composed of two

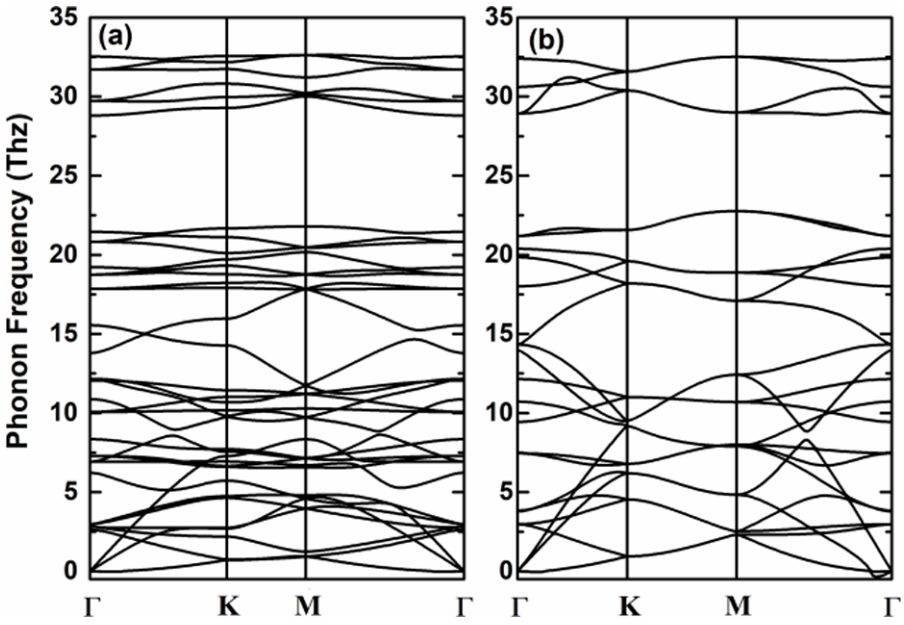

Figure 2. Phonon spectra of (a) H-AlN and (b) T-AlN monolayers.

graphene-like honeycomb AlN units connected by a pair of Al–N bonds. The bond lengths in the two graphene-like honeycomb units are 1.764 Å and 1.862 Å, and about 1.810 Å between the two graphene-like honeycombs. The T-AlN unit cell is an octagonal structure composed of one octagonal and one square unit. The octagonal unit has two alternate Al–N bonds with bond lengths of 1.832 Å and 1.764 Å, and a bond length of 1.832 Å between two octagonal units. Moreover, the theoretical surface areas of H-AlN and T-AlN can reach up to 2863 $m^2\ g^{-1}$ and 2615 $m^2\ g^{-1}$, which is comparable to the surface area of 2630 $m^2\ g^{-1}$ in graphene [43, 44].

To study the stability of the porous AlN monolayer, the formation energy was calculated. A lower formation energy indicates that the single layer is more stable and costs less energy to synthesize. The formation energy E_f of AlN monolayer is defined as

$$E_f = \frac{E_{monolayer}}{m} - \frac{E_{bulk}}{n}. \quad (1)$$

Here, E_{bulk} is the energy of bulk WZ-AlN structure and $E_{monolayer}$ is the energy of the porous monolayer. The numbers m and n are the number of Al–N pairs in porous monolayer and WZ-AlN, respectively. The formation energies of H-AlN, T-AlN, and g-AlN calculated using equation (1) are 1.47 eV, 1.32 eV, and 0.93 eV, respectively. Based on the same definition of formation energy, the formation energies are 1.52 eV and 1.98 eV per dimer for silicene and germanene, respectively [10, 45]. As silicene and germanene have already been experimentally fabricated on various substrates, these porous AlN monolayers may also be synthesized on appropriate substrates.

In order to investigate the structural stability of porous AlN monolayers, we next calculated the phonon spectrum using density functional perturbation theory. The results are shown in figure 2. It can be seen from the phonon dispersions that all the branches have positive frequencies in the entire Brillouin zone for both the H-AlN and T-AlN monolayers. No imaginary frequency components are present in the phonon spectra. This suggests that these two porous monolayers are dynamically stable free-standing 2D materials.

Although the dynamical stability of these H-AlN and T-AlN structures have been proven by the phonon spectrum analysis at $T = 0$ K, the structures may still be destroyed and transformed into other structures at high temperature. Hence, we have also examined the thermal stability using *ab initio* molecular dynamics simulations (AMDS). To avoid adverse effects from the periodic boundary condition, the AMDS used a $4 \times 4 \times 1$ supercell with contained 192 and 128 atoms for the H-AlN and T-AlN porous monolayers, respectively. The length of the time-step was chosen as 2 fs and simulations with 3000 steps were performed in a canonical ensemble (NVT) at constant temperature $T = 300$ K and 1300 K. The total potential energy per atom pair as a function of time-step and the structures at the end of the simulation for H-AlN and T-AlN at different temperatures are presented in figures 3(a)–(d), respectively. The final structures of both porous monolayers at the end of the AMDS are also shown in figure 3. From the figure, we can see that the total energies of the systems remain nearly constant and show only small deviations around the average energies during the simulation at 300 K. At the end of the simulation, the structures show no significant differences compared with the initial structures. Furthermore, a series of AMDS calculations were performed under different temperatures from 300 K to 1300 K at intervals of 200 K. The total energies of the systems show only small deviations around the average energies during the simulation process, even at 1300 K. The structures at the end of the simulation have small wrinkles of around 0.2–0.4 Å. The simulations show that the structures of H-AlN and T-AlN monolayers are not destroyed at 1300 K for 6 ps. This also indicates that the H-AlN and T-AlN monolayers are stable at high temperature. All of these suggest that the porous monolayers have excellent structural

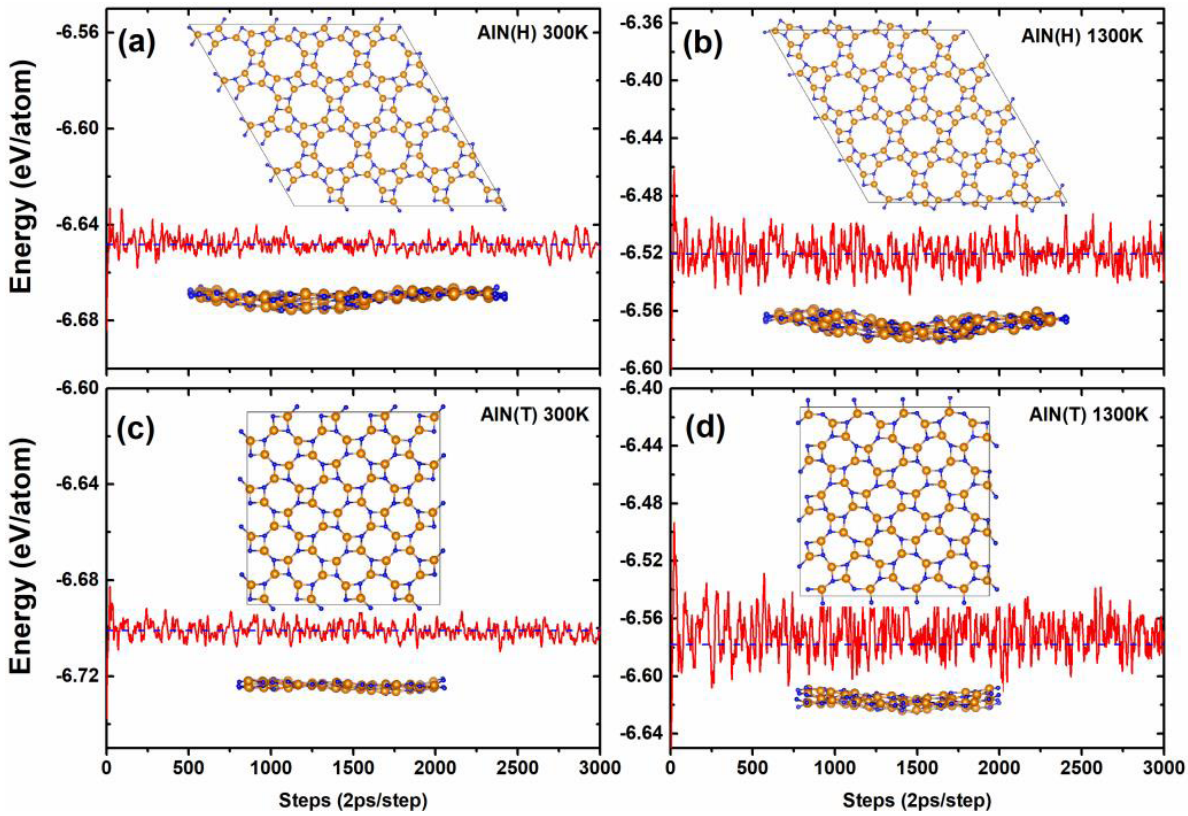

Figure 3. Relations between total energy and simulation time during the *ab initio* molecular dynamics simulations: (a) H-AlN at 300 K, (b) H-AlN at 1300 K, (c) T-AlN at 300 K, and (d) T-AlN at 1300 K. The AMDs were performed at $T = 300$ K and 1300 K at the last 6 ps. The structures at the end of the AMDs are also shown.

stability and can be synthesized experimentally at room temperature in the future.

3.2. Electronic structures

The electronic characteristics of the porous AlN monolayers were studied by using the GGA-PBE method. The band structures and the corresponding densities of states are shown in figures 4 and 5. Calculations were also performed for non-porous g-AlN monolayer and WZ-AlN for comparison. The results are consistent with previous studies [42]. As shown in figure 4, H-AlN, T-AlN, and g-AlN have indirect band structures while WZ-AlN does not. The indirect band gaps of the H-AlN and T-AlN monolayers are 2.89 eV and 2.86 eV respectively, close to the 2.91 eV of g-AlN. This indicates that the 2D monolayer materials may be useful for future optoelectronic applications.

In addition, the conduction band minimums (CBMs) are all located at the Γ point, but the valence band maximums (VBMs) are located at different points in the Brillouin zone. For the H-AlN monolayer, the VBM is located on the *K* point, while the VBM for T-AlN is on the K-Γ line. As shown in figure 5, the density of states analysis for the CBMs shows that they all originate from the *s* orbitals of both Al and N atoms. Furthermore, for both H-AlN and T-AlN, the densities of states suggest that the *p* orbitals of N atoms dominate the valence states near the Fermi level while those of the Al atoms play a less significant role. This is similar to other allotropes of AlN and group-III nitrides and is a common characteristic in most monolayer honeycomb structures [11], and can usually be attributed to the difference in the electronegativities of different atoms [46].

The screened hybrid function produces band gaps which agree much better with the experimental values for group-III nitrides compared to the band gaps obtained using GGA [47]. The hybrid-DFT method was adopted to evaluate the band gaps of the porous structures more accurately. Using the HSE06 functional with 25% Hartree–Fock exchange energy, the calculated band gap for WZ-AlN is 5.56 eV, which is consistent with the previously reported theoretical value [47]. This result agrees much better with previous experimental data (6.25 eV) than the GGA value (4.1 eV) [42, 47]. For H-AlN and T-AlN, the GGA calculation produced enlarged band gaps of 4.04 eV and 4.01 eV as shown with the red dashed lines in figures 4(a) and (b), respectively. However, despite the different magnitudes of the band gaps, the trends in the obtained band structures are similar to the GGA-PBE results. In addition, we would like to point out that although conventional DFT methods underestimate the band gaps in semiconductors, these methods have been proven to be effective in predicting the trends and physical mechanisms in previous works [7, 9, 48]. Therefore, the results which follow in this work are based on conventional DFT methods with the GGA-PBE scheme.

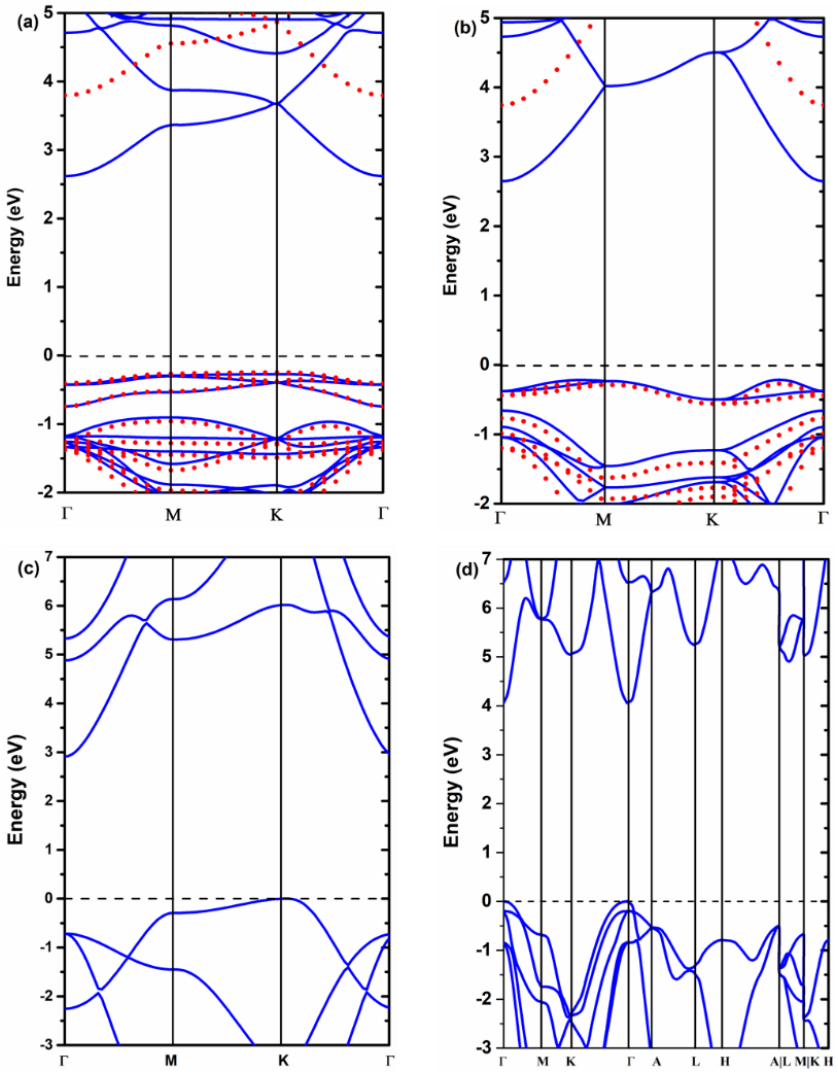

Figure 4. The band structures of (a) H-AlN and (b) T-AlN calculated with the GGA-PBE (blue) scheme. The red dashed lines in band structures (a) and (b) were obtained with the HSE06 scheme. The band structures of (c) g-AlN and (d) WZ-AlN calculated with the GGA-PBE (blue) scheme.

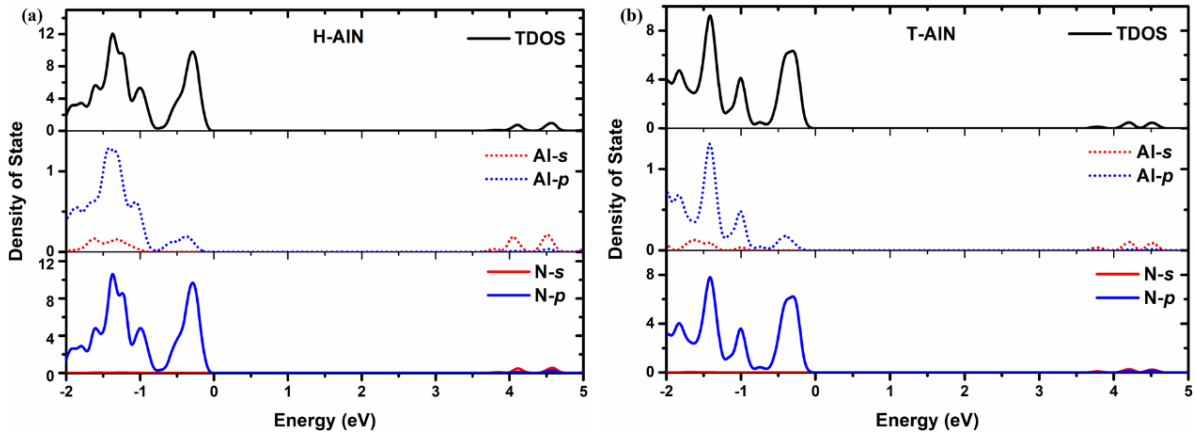

Figure 5. The densities of states of (a) H-AlN and (b) T-AlN calculated with the GGA-PBE scheme.

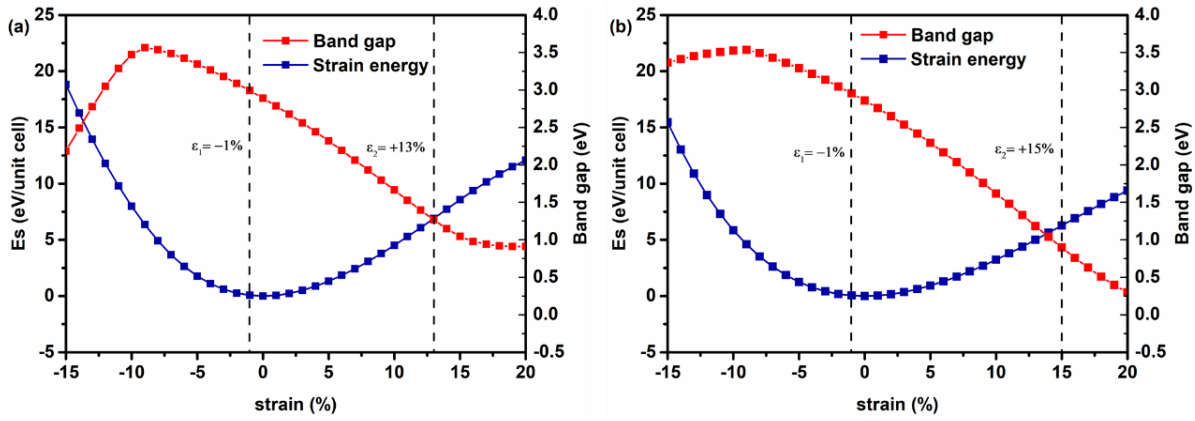

Figure 6. Strain energy and band gap of (a) H- and (b) T-AlN monolayer as functions of biaxial strains. ε_1 and ε_2 are the two critical strains obtained from the phonon spectrum calculations.

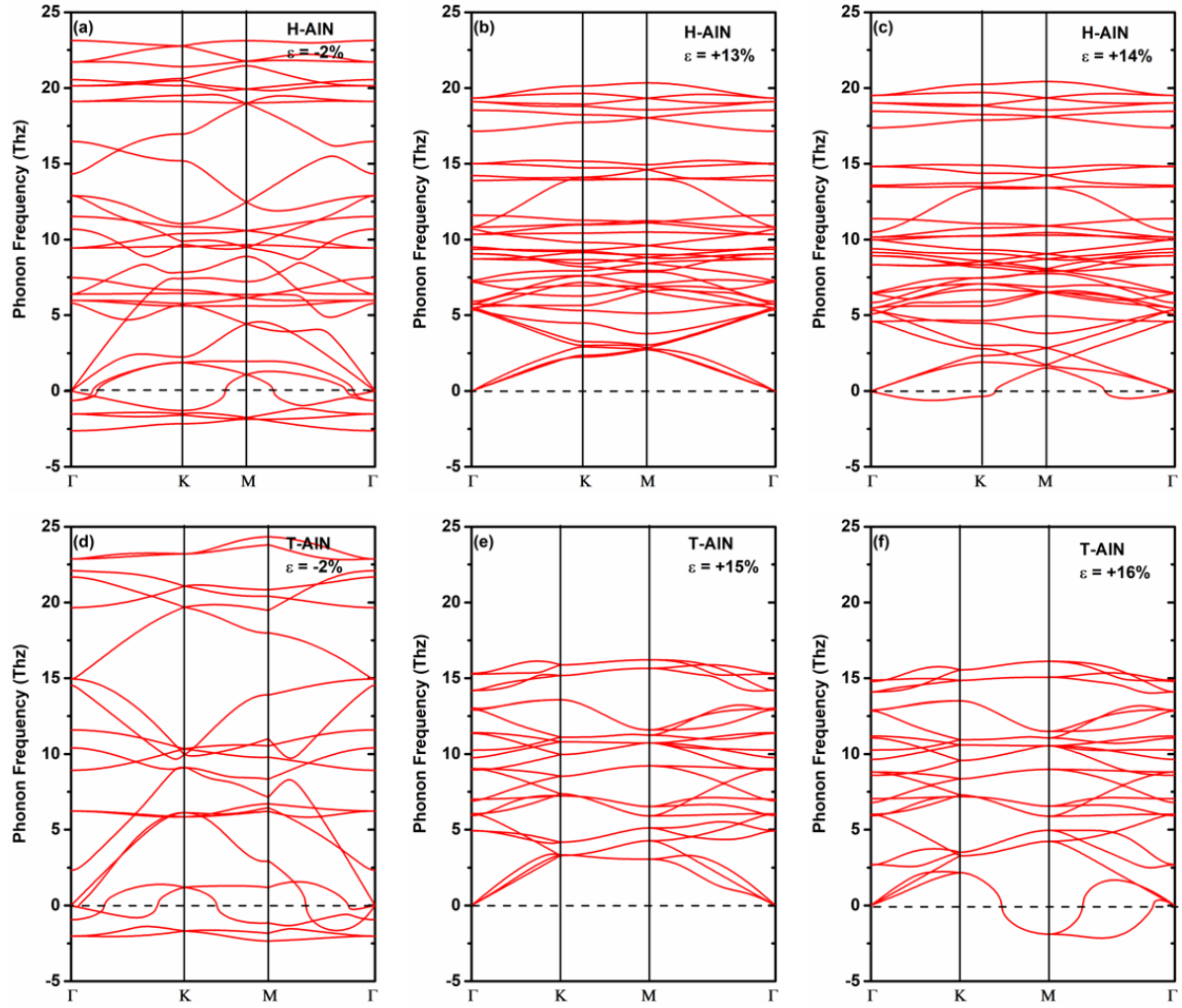

Figure 7. Phonon dispersion spectra of strained (a) H- and (b) T-AlN monolayer.

3.3. Strain effect on band gap tuning

As a common and effective method for tuning the electronic properties of semiconductors, in-plane strain has been extensively investigated through theoretical calculations. Due to their novel structures, 2D materials can withstand much larger strains than their corresponding bulk crystals [47, 49–52]. More precisely, changes in the bond lengths and confinement effects can modify the electronic structures. Thus, in order to obtain deeper insight into the electronic properties, biaxial compressive and tensile strains were applied to the AlN monolayers. The strain energy per unit cell is defined as

$$E_s = E_T(\varepsilon) - E_T(\varepsilon = 0) \quad (2)$$

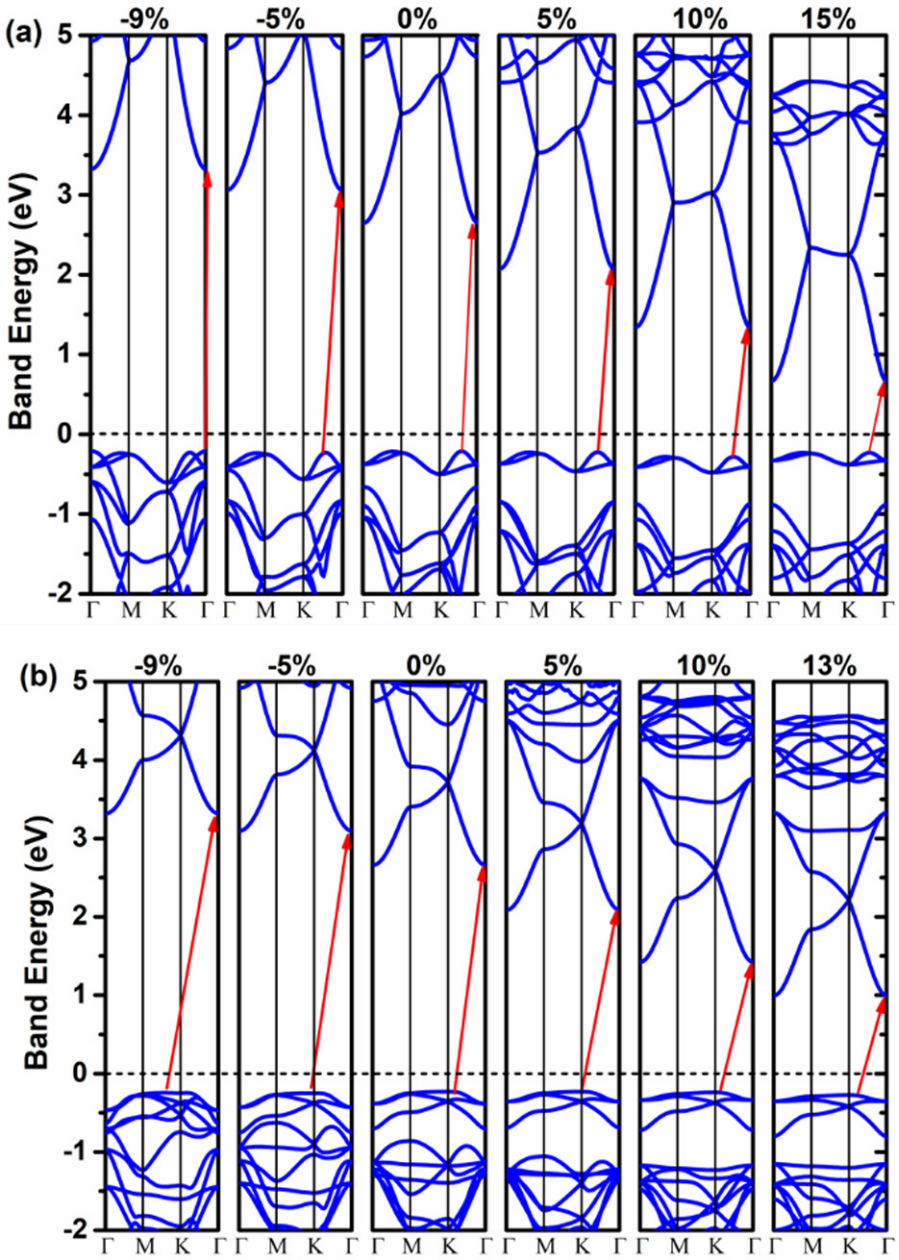

Figure 8. Band structures of (a) T- and (b) H-AlN monolayer under -9%, -5%, 0%, 5%, 10% and 15% biaxial strains.

where $\varepsilon = \frac{a-a_0}{a_0} \times 100\%$ with a_0 being the lattice constant at the equilibrium state, and a the lattice constant at the strained state. E_s, $E_T(\varepsilon)$, and $E_T(\varepsilon = 0)$ are the strain energy, the total energy at applied strain ε, and the total energy at the equilibrium states of a unit cell, respectively.

In order to obtain reliable results, biaxial strain was continuously applied to the AlN monolayers at intervals of 1%. The strain energies of H-AlN and T-AlN monolayers as functions of strain are presented in figure 6. The strain energies are nearly independent of the structure types and show similar trends within the imposed strain range. In both monolayers, the strain energies increase continuously with the strain without any sudden drops. A sudden drop in the strain energy usually indicates that the material is undergoing brittle fracture and local rupture. Although the application of strain results in large changes in the bond lengths and tetragonal unit cell shapes of structural optimized porous AlN monolayers, the monolayers do not decompose in the simulations. The monolayers may return to their initial shapes when the strain is released and the deformations disappear. Their unique structure plays an important role in the whole process. Similar behavior has also found in nitrogene monolayers [53], which undergo elastic deformation under strain. To further confirm the structural stability of the strained AlN monolayers, the phonon spectra of these strained monolayers were calculated, and shown in figure 7. As shown in figure 6, ε_1 and ε_2 are the two critical strains obtained from the phonon spectrum calculations. No imaginary frequency components are present when $\varepsilon_1 < \varepsilon < \varepsilon_2$, which suggests that the strained monolayers are dynamically stable in this strain range. Imaginary frequency components appear when the strain is increased to $\varepsilon > \varepsilon_2$ or $\varepsilon < \varepsilon_1$. In particular, the porous AlN monolayers are sensitive

to compressive strain. This behavior is similar to strained H-ScN monolayers, which are stable only when tensile strain is applied according to their phonon dispersion curves [54].

To further investigate the effects of strain, figure 6 shows the band gaps of strained porous AlN monolayers. As can be seen from the plots, the band gaps in both H-AlN and T-AlN vary with the strain. The band gaps can thus be tuned by applying strains. For tensile strain ($\varepsilon > 0$), the band gaps decrease monotonically while the strain is increased from -10% to $+15\%$. These results are similar to those in a previous study on g-GaN where the band gaps were reported to decrease linearly with the tensile strain [52]. The decrease in the band gap can be attributed to the modification of orbitals under strain. Under tensile strain, the bonds between neighboring atoms are stretched, and the electron distribution and the orbital hybridization will be modified to adapt to the changes. This eventually leads to changes in the band gaps. However, for compressive strain ($\varepsilon < 0$), the band gap increases and reaches the largest value of 3.56 (H-AlN) and 3.53 eV (T-AlN) as the compressive strain ($\varepsilon < 0$) increases from 0% to 9%. In conclusion, the band gap decreases under tensile strain while it increases to a maximum under moderate compressive strain and decreases again under extreme compressive strain. The band gaps of strained porous AlN monolayers show unique properties absent in other 2D monolayers like germanene and phosphorene [50, 55].

More interestingly, there is a direct–indirect band gap transition in the T-AlN monolayer under strain. The electronic band structures under different strains for T-AlN and H-AlN were calculated, and illustrated in figure 8. Our results indicate that unstrained H-AlN and T-AlN monolayers are indirect band gap semiconductors. The CBM of the porous monolayers are always located at the Γ point. However, the VBM varies along the Γ-M-K-Γ path in the 2D Brillouin zone. As can be seen from the figures, an increase in the compressive strain from -0% to -9% leads to a direct–indirect transition in T-AlN. The VBM of T-AlN moves to the Γ point at -9% strain, which results in a direct–indirect transition, as shown in figure 8. When the compressive strain is increased further, the VBM shifts away from the Γ point to the K-Γ line and T-AlN transforms into an indirect band gap semiconductor again. Although the T-AlN monolayer becomes a direct band gap semiconductor at –9% strain, the H-AlN monolayer remains an indirect band gap semiconductor for all applied strain values.

These findings may be due to the following reasons. Firstly, the shortening of the bond length may play an important role in the direct–indirect band gap transition. Under compressive strain, the bond lengths between the neighboring atoms are shortened. The compressive strain leads to increased repulsion between the orbitals and has different impacts on the in-plane and out-of-plane orbitals. This reorganizes the bands near the Fermi level and causes the VBM shifts [56]. The proximity orbital energies of N-2*p* (8.4 eV) and Al-3*s* (8.0 eV) are probably a second factor [46]. Due to the short bond lengths and the proximity orbital energies in both allotropes, the N-2*p* and Al-3*s* orbitals form hybrid orbitals that change the valence states near the Fermi level.

4. Conclusion

In conclusion, two novel porous AlN monolayers were explored with density functional theory under the general gradient approximation expressed using the PBE functional. Their stabilities were demonstrated by the phonon dispersion spectra and the molecular dynamics simulations. The results show that these porous monolayers have excellent structural stability and can withstand temperatures as high as 1300 K. Based on our findings, we performed a systematic investigation of the electronic structures of these monolayers. Our results indicate that the H- and T-AlN monolayers are indirect-gap semiconductors with band gaps of 2.89 eV and 2.86 eV in the absence of strain. Moreover, we showed that the electronic structures can be modulated by strain. For T-AlN, there is an indirect–direct band gap transition under compressive strain. Because of their unique porous structures, large surface areas, and tunable bandgaps, these two monolayer materials may potentially be used in future optoelectronic and catalyst applications.

Acknowledgments

This work was supported by the National Basic Research Program of China (Grant No. 2012CB921300), the National Natural Science Foundation of China (Grant No. 11274280), the Foundation of Henan Educational Committee (Grant No. 20A140009), and the Scientific Foundation of Henan University of Technology (Grant No. 2018BS039). The calculations were supported by the High Performance Computing Center of Zhengzhou University, Zhongyuan University of Technology, and Zhengzhou Normal University.

ORCID iDs

Yanwei Luo https://orcid.org/0000-0002-5316-9147

References

[1] Novoselov K S, Geim A K, Morozov S V, Jiang D, Zhang Y, Dubonos S V, Grigorieva I V and Firsov A A 2004 *Science* **306** 666
[2] Zhang Y, Tan Y W, Stormer H L and Kim P 2005 *Nature* **438** 201
[3] Wang Q H, Kalantar-Zadeh K, Kis A, Coleman J N and Strano M S 2012 *Nat. Nanotechnol.* **7** 699
[4] Alem N, Erni R, Kisielowski C, Rossell M D, Gannett W and Zettl A 2009 *Phys. Rev.* B **80** 155425
[5] Li L, Yu Y, Ye G J, Ge Q, Ou X, Wu H, Feng D, Chen X H and Zhang Y 2014 *Nat. Nanotechnol.* **9** 372
[6] Xia F, Wang H and Jia Y 2014 *Nat. Commun.* **5** 4458
[7] Luo Y W, Li Y X, Wang F, Guo P and Jia Y 2017 *Physica* E **94** 64
[8] Luo Y W, Zhang S, Chen W G and Jia Y 2018 *Phys. B: Condens. Matter* **534** 51
[9] Liu H, Neal A T, Zhu Z, Luo Z, Xu X, Tomanek D and Ye P D 2014 *ACS Nano* **8** 4033

[10] Zheng H, Li X B, Chen N K, Xie S Y, Tian W Q, Chen Y, Xia H, Zhang S B and Sun H B 2015 *Phys. Rev.* B **92** 115307
[11] Kamal C, Chakrabarti A and Ezawa M 2016 *Phys. Rev.* B **93** 125428
[12] Singh A K and Hennig R G 2014 *Appl. Phys. Lett.* **105** 042103
[13] Kang J, Li J, Wu F, Li S S and Xia J B 2011 *J. Phys. Chem.* C **115** 20466
[14] Su J, Zou X, Li G D, Jiang Y M, Cao Y, Zhao J and Chen J S 2013 *Chem. Commun.* **49** 8217
[15] Zdravkov B, Čermák J, Šefara M and Janků J 2007 *Open Chem.* **5** 385
[16] Liang C, Li Z and Dai S 2008 *Angew. Chem., Int. Ed.* **47** 3696
[17] Dai J, Li M and Zeng X C 2016 *WIREs Comput. Mol. Sci.* **6** 211
[18] Dai J, Wu X, Yang J and Zeng X C 2014 *J. Phys. Chem. Lett.* **5** 2058
[19] Bieri M *et al* 2009 *Chem. Commun.* **45** 6919
[20] Liu Y, Wang G, Huang Q, Guo L and Chen X 2012 *Phys. Rev. Lett.* **108** 225505
[21] Dai J, Wu X, Yang J and Zeng X C 2014 *J. Phys. Chem. Lett.* **5** 393
[22] Wen B, Zhao J, Melnik R and Tian Y 2011 *Phys. Chem. Chem. Phys.* **13** 14565
[23] Ma Z, Han Z, Liu X, Yu X, Wang D and Tian Y 2017 *Nanomaterials* **7** 3
[24] Li P and Luo W 2016 *Sci. Rep.* **6** 25423
[25] Şahin H, Cahangirov S, Topsakal M, Bekaroglu E, Akturk E, Senger R T and Ciraci S 2009 *Phys. Rev.* B **80** 155453
[26] Bourret A, Barski A, Rouviere J, Renaud G and Barbier A 1998 *J. Appl. Phys.* **83** 2003
[27] Ponce F and Bour D 1997 *Nature* **386** 351
[28] Strite S and Morkoç H 1992 GaN, AlN and InN: a review *J. Vac. Sci. Technol.* B **10** 1237
[29] Morkoç H, Strite S, Gao G B, Lin M E, Sverdlov B and Burns M 1994 *J. Appl. Phys.* **76** 1363
[30] Li J, Nam K, Nakarmi M, Lin J, Jiang H, Carrier P and Wei S H 2003 *Appl. Phys. Lett.* **83** 5163
[31] Jain S, Willander M, Narayan J and Overstraeten R V 2000 *J. Appl. Phys.* **87** 965
[32] Ozgit C, Donmez I, Alevli M and Biyikli N 2012 *Thin Solid Films* **520** 2750
[33] Nepal N, Anderson V R, Hite J K and Eddy C R 2015 *Thin Solid Films* **589** 47
[34] Yan X, Dong Y, Li H, Gong J and Sun C 2010 *Mater. Lett.* **64** 1261
[35] Alizadeh M, Goh B T and Rahman S A 2017 *Metall. Mater. Trans.* A **48** 3461
[36] Kresse G and Furthmüller J 1996 *Comput. Mater. Sci.* **6** 15
[37] Kresse G and Hafner J 1993 *Phys. Rev.* B **47** 558
[38] Blochl P E 1994 *Phys. Rev.* B **50** 17953
[39] Perdew J P, Burke K and Ernzerhof M 1996 *Phys. Rev. Lett.* **77** 3865
[40] Zhang W X, Li T, Gong S B, He C and Duan L 2015 *Phys. Chem. Chem. Phys.* **17** 10919
[41] Valedbagi S, Fathalian A and Elahi S M 2013 *Opt. Commun.* **309** 153
[42] Vogel D, Krüger P and Pollmann J 1997 *Phys. Rev.* B **55** 12836
[43] Zhu Y, Murali S, Cai W, Li X, Suk J W, Potts J R and Ruoff R S 2010 *Adv. Mater.* **22** 3906
[44] Xu Y, Lin Z, Zhong X, Huang X, Weiss N O, Huang Y and Duan X 2014 *Nat. Commun.* **5** 4554
[45] Zhang H L and Hennig R G 2014 *JOM* **66** 366
[46] Litimein F, Bouhafs B, Dridi Z and Ruterana P 2002 *New J. Phys.* **4** 64
[47] Yan Q M, Rinke P and Scheffler M 2009 *Appl. Phys. Lett.* **95** 121111
[48] Zhang S, Yan Z, Li Y, Chen Z and Zeng H 2015 *Angew. Chem. Int. Ed.* **54** 3112
[49] Peelaers H and Van de Walle C G 2012 *Phys. Rev.* B **86** 241401
[50] Peng X, Wei Q and Copple A 2014 *Phys. Rev.* B **90** 085402
[51] Choi S M, Jhi S H and Son Y W 2010 *Phys. Rev.* B **81** 081407
[52] Kim K, Lambrecht W R and Segall B 1996 *Phys. Rev.* B **53** 16310
[53] Li J S, Wang W L and Yao D X 2016 *Sci. Rep.* **6** 34177
[54] Tamleh S, Rezaei G, Vaseghi B and Jalilian J 2019 *J. Phys. Chem. Solids* 109270
[55] Yan J A, Gao S P, Stein R and Coard G 2015 *Phys. Rev.* B **91** 245403
[56] Kecik D, Bacaksiz C, Senger R T and Durgun E 2015 *Phys. Rev.* B **92** 165408